

# Mechanical and Geophysical Monitoring of Slip Along Frictional Discontinuities

El Fil, H

*Lyles School of Civil Engineering, Purdue University, West Lafayette, IN, USA*

Bobet, A

*Lyles School of Civil Engineering, Purdue University, West Lafayette, IN, USA*

Pyrak-Nolte, L.J.

*Department of Physics, Department of Earth and Atmospheric Sciences, Lyles School of Civil Engineering, Purdue University, West Lafayette, IN, USA*

Copyright 2019 ARMA, American Rock Mechanics Association

This paper was prepared for presentation at the 53<sup>rd</sup> US Rock Mechanics/Geomechanics Symposium held in New York, NY, USA, 23–26 June 2019. This paper was selected for presentation at the symposium by an ARMA Technical Program Committee based on a technical and critical review of the paper by a minimum of two technical reviewers. The material, as presented, does not necessarily reflect any position of ARMA, its officers, or members. Electronic reproduction, distribution, or storage of any part of this paper for commercial purposes without the written consent of ARMA is prohibited. Permission to reproduce in print is restricted to an abstract of not more than 200 words; illustrations may not be copied. The abstract must contain conspicuous acknowledgement of where and by whom the paper was presented.

**ABSTRACT:** Shear strength along discontinuities plays a crucial role in the stability of rock structures. The development of geophysical methods to remotely monitor and assess changes in shear strength is essential to the identification of rock hazards that can lead to the loss of life and failure of civilian infrastructure. In this study, compressional and shear ultrasonic waves were used to monitor slip along discontinuities (with different surface profiles) during shearing. A series of laboratory direct shear experiments was performed on two gypsum blocks separated by a frictional discontinuity. The gypsum blocks had perfectly matched contact surfaces with a half-cycle sine wave profile that spanned the central third of the discontinuity, surrounded by planar surfaces. The amplitude of the half-cycle sine wave was varied and ranged between 2 to 10 times the height of the asperities. Compressional, P, and shear, S, ultrasonic waves were continuously transmitted and recorded throughout the shearing process, while Digital Image Correlation (DIC) was used to capture surface displacements. At low normal stresses, distinct maxima in the normalized P and S wave transmitted amplitudes occurred before shear failure in regions where dilation was observed. Where dilation was not detected, an increase in transmitted wave amplitude was observed, even after the peak shear stress was achieved. At high normal stresses, dilation was suppressed, which was associated with an increase in wave amplitude with shear stress until the peak, and then a decrease in amplitude. Monitoring changes in transmitted wave amplitude is a potential method for the detection of dilation along rock discontinuities.

## 1. INTRODUCTION

Pre-existing discontinuities in a rock mass are often subjected to compressive and shear loads. The shear strength of rock joints depends on the level of effective normal stress applied on the plane of sliding, the rock type, the roughness of the joint surface, the size of the joint (scale effects), the slip rate and the environmental conditions, i.e. fluids and pore pressure (Byerlee, 1978; Jaeger et al., 2007; Hoek, 2007 and 2018). Shear strength along rock discontinuities is a concern in many rock engineering applications such as stability of underground excavations and slope stability of rock masses. Thus, determining the shear strength of rock joints is critical and can significantly affect the safety of structures in and on rock (Zhao, 1997a).

Laboratory small-scale direct shear tests enable controlled examination of different mechanisms that affect the shear strength of joints. In this research, we examine the effect of fracture surface profile on the behavior of a discontinuity during shearing, and whether slip (with and

without dilation) affects transmitted compressional and shear elastic waves. The significance of the shape of the surface profile was first highlighted by Patton (1966). He proposed a failure criterion that considers either shearing off the asperities, shearing along the asperities, or both. Barton and Choubey (1977) proposed an empirical criterion for rock joints that can be used to predict the shear strength. The empirical criterion is based on the joint roughness coefficient (JRC), the joint wall compressive strength (JCS), and the residual friction angle. Various shear failure criteria for rock discontinuities have been developed over the years (Barton, 1973; Barton and Choubey, 1977; Kulatilake et al., 1995; Homand et al., 2001; Xia et al., 2014). All these studies are based on two assumptions that are not necessarily true: (1) the shear resistance along the discontinuity is uniform; (2) the normal stress is uniformly distributed along the interface. Several researchers found that slip along a discontinuity starts from an area with low frictional resistance and then extends to areas with higher frictional resistance (Mutlu and Bobet, 2006; Hedayat et al. 2014).

Mechanical monitoring of shear failure is important, yet geophysical techniques can also be used to remotely probe the discontinuity that is being sheared. Active seismic monitoring has been used as a successful technique to locate discontinuities (Modiriasari et al., 2015), assess the state of the stress along discontinuities (Kendall and Tabor, 1971; Schoenberg, 1980) and provide information about the engineering properties of discontinuities such as stiffness (Choi et al., 2014). In addition, active monitoring with transmitted and reflected compressional, P, and shear, S, waves has been used to detect crack initiation, propagation and coalescence (Modiriasari et al., 2017).

The aim of this study is to determine the role of a discontinuity profile in generating slip with and without dilation, and if compressional, P, and shear, S, waves can detect both modes of slip.

## 2. SPECIMEN PREPARATION AND EXPERIMENTAL SETUP

### 2.1. Direct Shear Experiments

A series of laboratory direct shear experiments was conducted on gypsum specimens, each containing a single discontinuity. The specimens consisted of two independent prismatic blocks with dimensions 152.4 mm long, 127 mm wide and about 50.8 mm thick. The gypsum material was made from a mixture of gypsum, diatomaceous earth, and water, with the following mass proportions: water/gypsum = 0.4; water/diatomaceous earth = 35.0. The specimens were cast in two steps: (1) a prismatic gypsum block was cast against a grit 36 sand paper to create a rough discontinuity; and (2) after the first block hardened, a second block was cast against the first block to create a two-piece assembly with a perfectly mated interface.

Laser profilometry was used to measure the surface roughness of the discontinuities prior to shearing. Fig. 1 shows the probability distribution of asperity heights from one of the cast surfaces. The asperity heights exhibit a normal distribution with a minimum height of -0.39 mm and a maximum of 0.32 mm, with a standard deviation of 0.132 mm.

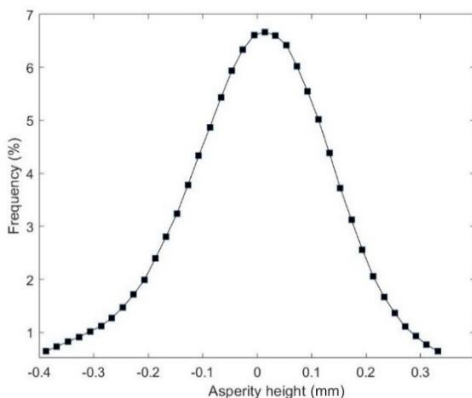


Fig. 1. Frequency distribution of the height of the asperities

Two types of contact surfaces were prepared: (1) flat, to investigate the shear strength of the interface; and (2) with half-cycle sine wave that spanned the central 1/3 of the discontinuity length (see Fig. 2 and Fig. 6) to determine the effect of fracture profile on joint dilation during shearing. 3D printing was used to create plastic prismatic blocks with specific surface profiles. Several plastic blocks were printed to create molds with surface profiles that contained a half-cycle central sine wave with different amplitudes (Fig. 6). The amplitudes ranged between 0.6 to 3.2 mm, which are 2 - 10 times greater than the maximum asperity height created with the sand paper (Fig. 1).

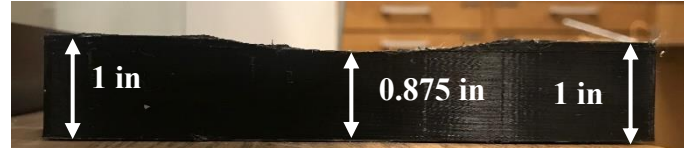


Fig. 2. 3D Printed mold-base for specimens with a half-cycle sine wave of amplitude 0.125 in (3.2 mm, an order of magnitude larger than the height of the asperities)

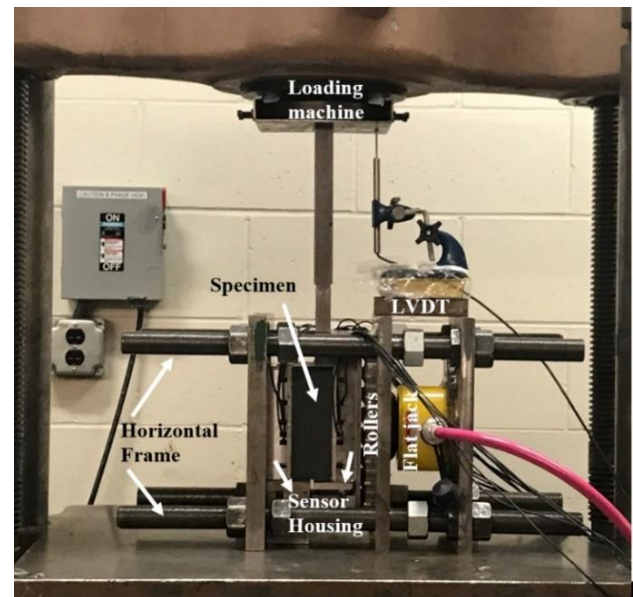


Fig. 3. Experimental setup

A direct shear apparatus (Fig. 3) was used, that consisted of a horizontal loading frame to apply a normal stress on the joint and a separate loading machine to apply a shear load. The horizontal frame was composed of a flat-jack, loading platens, steel rods, rollers and plates. A series of rollers was positioned between one of the loading platens and the steel plate to minimize the vertical friction. The direct shear experiments were run under a normal load of 1 or 2 MPa, and with a shearing rate of  $8\mu\text{m/s}$ . A linear variable differential transformer (LVDT) was used to record the average vertical displacement of the specimen. An electronic feedback loop was used to control the flat-jack pressure to ensure that the normal load remained constant throughout the experiment. Compressional, P, and shear, S, ultrasonic waves were transmitted across the

specimens during the experiments. The ultrasonic sensor arrays were housed inside the load platens (Fig. 3). Two sensor arrays (receivers and source arrays in Fig. 4) were used, each with 9 embedded ultrasonic transducers. Fig. 4(a) shows a schematic of the experimental setup and the transducer layout.

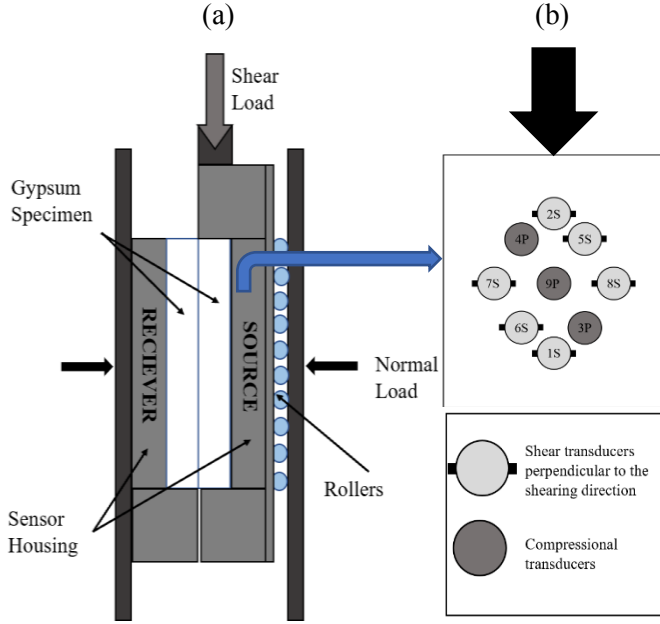


Fig. 4. (a) Schematic of the setup; (b) transducers layout

The transducers were coupled to the surface of the specimens using oven-baked honey (90 minutes at 90 °C). Then, a 1 MPa normal stress was applied to the specimen and platens that housed the transducers. The load was maintained for 4 hours before testing to ensure that the coupling between transducers and specimen reached a stable condition. After 4 hours, the specimen was loaded up to the desired normal stress and then a shear load was applied using a constant rate of displacement. Shear loading continued until about 1 mm of displacement occurred after reaching peak shear load.

## 2.2. Digital Image Correlation (DIC)

Digital image correlation (DIC) was used in this study to monitor fracture displacement during shearing. DIC calculates the displacement field by comparing the digital images taken before and after deformation. DIC tracks the displacement by matching digital images taken throughout the experiment. The first image is used as the reference image which is the basis for computing the surface displacements. A target pixel, or point of interest, is tracked from the reference image to the subsequent images of the deformed surface (from point  $S$  to point  $T$  in Fig. 5) (Sutton et al., 2009). A square subset, with the target pixel at its center, is used for the analysis to aid in the identification of the target pixel. It has a size of  $2M+1$  pixels around the point of interest, as seen in Fig. 5, which also shows a schematic on the matching process around the point of interest  $S(f(x_i, y_j))$ .

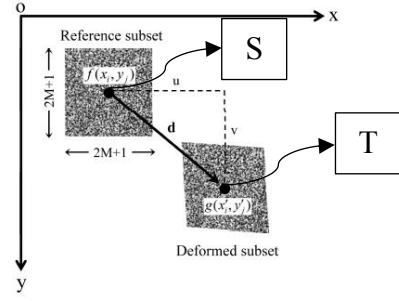


Fig. 5. Referenced and deformed subsets used in DIC (Pan et al., 2009)

A degree of similarity is defined by a correlation criterion created between the reference subset and the deformed images. The two most frequently used criteria in DIC are the Cross-Correlation criteria (CC) and the Sum of Square Differences criteria (SSD) (Giachetti, 2000; Sutton et al., 2008; Pan et al., 2009). Both criteria are given in three forms: (1) their original form (either CC or SSD), (2) their normalized form (NCC or NSSD), and (3) their zero normalized form (ZNCC or ZNSSD). The most accurate results are obtained from the zero normalized form because it is insensitive to any offset in the illumination lighting and pixel intensity values, and reduces data noise (Pan et al., 2009). In this paper, the zero normalized form (ZNCC) is used to analyze surface displacements from DIC images.

$$C_{ZNCC(d)} = \sum_{i=-M}^M \sum_{j=-M}^M \left[ \frac{(f(x_i, y_j) - f_m)(g(x'_i, y'_j) - g_m)}{\Delta f \Delta g} \right] \quad (1)$$

In Eq. (1),  $f(x_i, y_j)$  is the pixel intensity at coordinate  $(x_i, y_j)$  (point  $S$  in Fig. 5) of the reference subset in the reference image, and  $g(x'_i, y'_j)$  is the pixel intensity at coordinate  $(x'_i, y'_j)$  (point  $T$ ) of the deformed subset in the deformed image. Where,

$$f_m = \frac{1}{(2M+1)^2} \sum_{i=-M}^M \sum_{j=-M}^M f(x_i, y_j) \quad (2)$$

$$g_m = \frac{1}{(2M+1)^2} \sum_{i=-M}^M \sum_{j=-M}^M g(x'_i, y'_j) \quad (3)$$

$$\Delta f = \sqrt{\sum_{i=-M}^M \sum_{j=-M}^M (f(x_i, y_j) - f_m)^2} \quad (4)$$

$$\Delta g = \sqrt{\sum_{i=-M}^M \sum_{j=-M}^M (g(x'_i, y'_j) - g_m)^2} \quad (5)$$

The ZNCC criterion varies between 0 and 1. A value of 1 is associated with no difference in intensity of pixels between the reference and the deformed subset. The change in the location of the center point between the reference and the deformed subset defines the displacement vector  $d$ , as shown in Fig. 5. The same process is repeated for other grid points in the ROI to attain the full displacement field (Pan et al., 2009).

### 3. RESULTS AND DISCUSSION

Direct shear experiments were conducted on several specimens with frictional discontinuities with different surface profiles. Table 1 presents a summary of the tests performed with the corresponding profiles shown in Fig 6.

Table 1. Tests performed

Planar	Half-Cycle Sine Wave Amplitude= 0.025 in	Half-Cycle Sine Wave Amplitude= 0.05 in	Half-Cycle Sine Wave Amplitude= 0.125 in
$\sigma_n = 1 \text{ MPa}$ G_1_0	$\sigma_n = 1 \text{ MPa}$ G_1_.025	$\sigma_n = 1 \text{ MPa}$ G_1_.05	$\sigma_n = 1 \text{ MPa}$ G_1_.125
$\sigma_n = 2 \text{ MPa}$ G_2_0	$\sigma_n = 2 \text{ MPa}$ G_2_.025	$\sigma_n = 2 \text{ MPa}$ G_2_.05	$\sigma_n = 2 \text{ MPa}$ G_2_.125

All profiles consisted of two planar portions adjacent to a centrally-located half-cycle sine wave (Fig. 6). The amplitudes of the half-cycle sine wave for different specimens were 0 (planar), 0.6, 1.3, and 3.2 mm.



Fig. 6. A schematic of surface profiles for the prepared samples; from top to bottom (planar, G\_.025, G\_.05, G\_.125), respectively.

#### 3.1. Low Normal Stress

Experiments were conducted first at low normal stress (Table 1). For a planar surface profile (specimen G\_1\_0), the measured response in peak-to-peak transmitted wave amplitude (Fig. 7) was similar to that observed by Hedayat et al. (2014). Fig. 7 contains normalized transmitted wave amplitude for three representative transducers (5S, 9P and 1S) and the shear stress as a function of shear displacement. The representative transducers were chosen from the top (5S), middle (9P), and lower portion of the sample (1S). As observed in Fig. 7, the normalized transmitted amplitude increases with increasing shear stress and reaches a peak in transmission prior to failure at the peak load. The peak in transmission was identified as a precursor to failure by Hedayat et al. (2014) and is observed for sample G\_1\_0. The increase in amplitude is associated with an increase in the shear stiffness of the interface, which occurs as the asperities lock together. Once damage occurs, the amplitude decreases as the stiffness of the interface decreases.

Fig. 8 contains contour plots of vertical displacements at the peak load (21. MPa). Fig. 8(a) shows the displacements over the entire specimen. As the applied

the peak load (2.1 MPa), slip propagated along the discontinuity. Vertical displacements along the horizontal cross sections ( $y=25 \text{ mm}$ ,  $y=75 \text{ mm}$ , and  $y=125 \text{ mm}$ ) are presented in Fig. 8(b), where a discontinuity, i.e. “jump”, in displacement is clearly observed across the interface. No dilation along the interface was observed during the experiment.

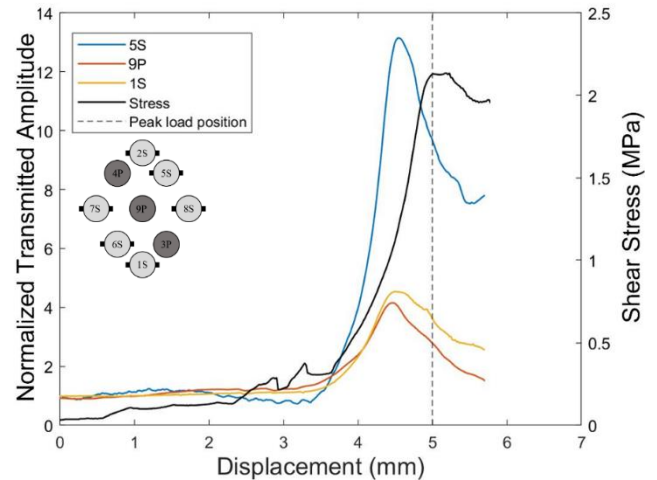


Fig. 7. Shear-stress vs. shear displacement and normalized transmitted amplitude for specimen G\_1\_0, showing representative transducers from top, middle and bottom portion of the sample. The dashed line indicates the displacement at which peak load was obtained (shear stress to normal stress ratio=2.1).

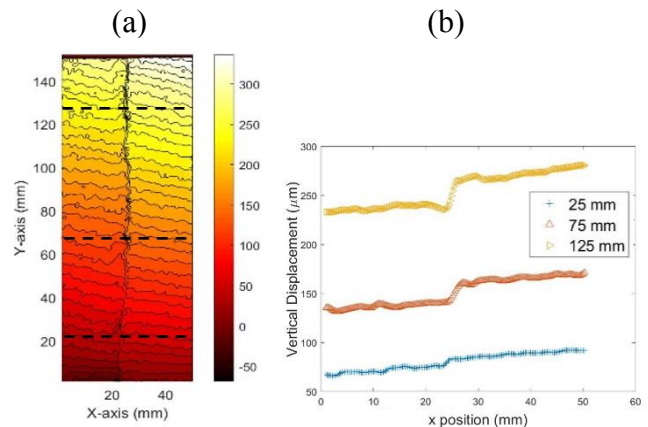


Fig. 8. Specimen G\_1\_0: (a) vertical displacements at peak load; (b) vertical displacements at different horizontal cross-sections

The ultrasonic and load-displacements results from specimens with non-planar surfaces are shown Fig. 9 and Fig. 10 for specimens G\_1\_.025 and G\_1\_.05, respectively. In Fig. 9 and 10, normalized transmitted wave amplitudes are shown for the same three representative transducers, top (5S), middle (9P) and bottom (1S) portion of the sample. The data in both figures indicate that the normalized transmitted P and S wave amplitudes increase as the shear stress increases, which is associated with an increase in contact among the asperities. The signal amplitude decreased as the

asperities were damaged. It can be observed that the results from specimens with a half-cycle sine wave amplitude of 0.6 and 1.3 mm were similar to those of the specimens with a planar discontinuity (specimen G\_1\_0); that is, the presence of a half-cycle sine wave that has an amplitude of the same order as the size of the asperities did not affect the P or S-wave precursors prior to peak load. The second order asperity, i.e. the half-cycle sine wave, had no effect on the shear behavior of the discontinuity when the maximum amplitude of the surface profile was less than the maximum surface asperity height. It is hypothesized that when the amplitude of the half-cycle sine wave is small, it is sheared along with the first order asperities that were created by casting gypsum against the sand paper.

Most of the transducers recorded precursors to failure. The appearance of the precursors relative to the peak displacement heavily depends on the damage induced to the asperities, which can vary spatially over the joint interface.

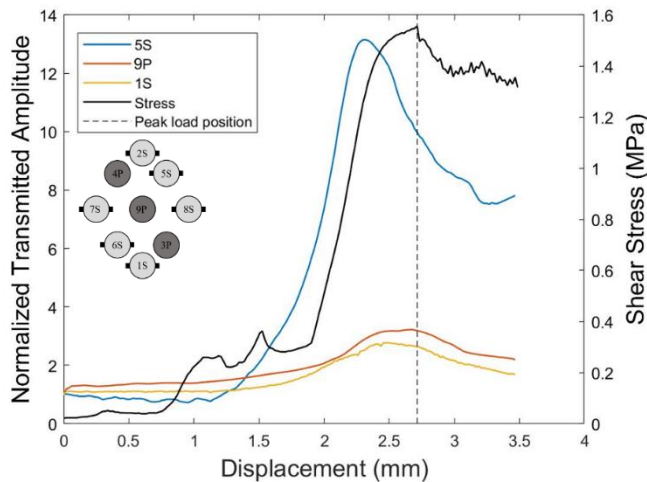


Fig. 9. Shear-stress vs. shear displacement and normalized transmitted amplitude for specimen G\_1\_025, showing representative transducers from top, middle and bottom portion of the sample (shear stress to normal stress ratio=1.58).

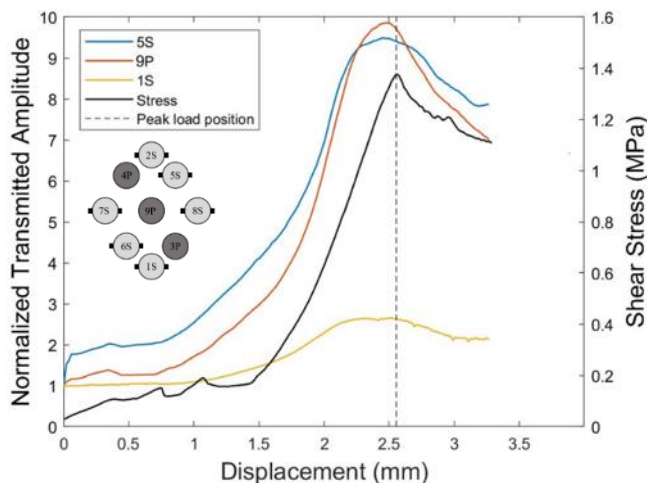


Fig. 10. Shear-stress vs. shear displacement and normalized

transmitted amplitude for specimen G\_1\_05, showing representative transducers from top, middle and bottom portion of the sample (shear stress to normal stress ratio=1.37).

The surface profile of specimen G\_1\_125 contained a central half-cycle sine wave with a maximum amplitude of 3.2 mm that was 10 times the maximum asperity height. Fig. 11 shows the normalized peak-to-peak amplitude of transmitted P and S waves for representative transducers, top (5S), middle (9P), and bottom (1S), and includes the shear stress as a function of the shear displacement. For the transducer at the top of the sample (5S), the normalized amplitude increased with increasing shear stress and continued to increase as the asperities were sheared (post peak failure). This is in contrast with the data from the transducers located at the middle and bottom of the specimen, which exhibited a drop in normalized amplitude post-peak (9P and 1S). At low normal stresses, distinct peaks in the transmitted amplitude occurred for transducers located where dilation was observed (middle and bottom). Where dilation was not detected (top of the specimen), the transducers recorded an increase in transmitted amplitude, even after the peak shear stress. Precursors to failure were not observed in any of the transmitted wave amplitudes. As shown in Fig. 11, the peaks of the normalized transmitted amplitude did not occur prior to the peak of the shear strength (1S).

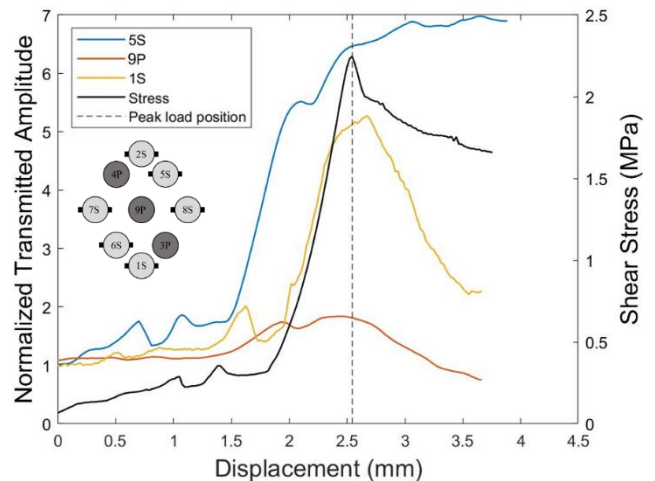


Fig. 11. Shear-stress vs. shear displacement and normalized transmitted amplitude for specimen G\_1\_125, showing representative transducers from top, middle and bottom portion of the sample (shear stress to normal stress ratio=2.38).

Fig. 12(a) and (c) show contour plots of vertical and horizontal displacements recorded at peak load (2.38 MPa), respectively. Vertical displacements along the horizontal cross sections ( $y=25$  mm,  $y=75$  mm, and  $y=125$  mm) are presented in Fig. 12(b). The discontinuity in vertical displacement (slip) is clearly seen in all horizontal sections. Fig. 12(c) is a contour plot of the horizontal displacement. Fig. 12(d) shows the horizontal

displacement profiles along all three horizontal sections. From the horizontal displacement measurements, dilation occurs at all heights along the length of the specimen. The dilatation is relatively small at  $y=125$  mm. The two blocks are in tight contact at the top of the specimen, but move apart at the bottom, as shown in Fig. 12(d). This is the result of a relative rotation of the two blocks that causes the blocks to separate at the bottom. This mechanism is consistent with the normalized transmitted amplitudes that show an increase in amplitude at the top and a decrease at the middle and bottom of the specimen (Fig. 11). It is hypothesized that the changes in amplitude of the transmitted waves are caused by two mechanisms: (1) the asperities are damaged and so the shear stiffness of the interface decreases, which induces a decrease in amplitude of the transmitted waves; (2) at the top, the normal contact stress between the two blocks increases due to the rotation, which in turn increases the normal and shear stiffness of the discontinuity, thus increasing the amplitude of the transmitted waves. At the bottom of the specimen, the effect is opposite: the normal stress decreases because of the rotation, which induces an additional reduction in transmitted wave amplitude.

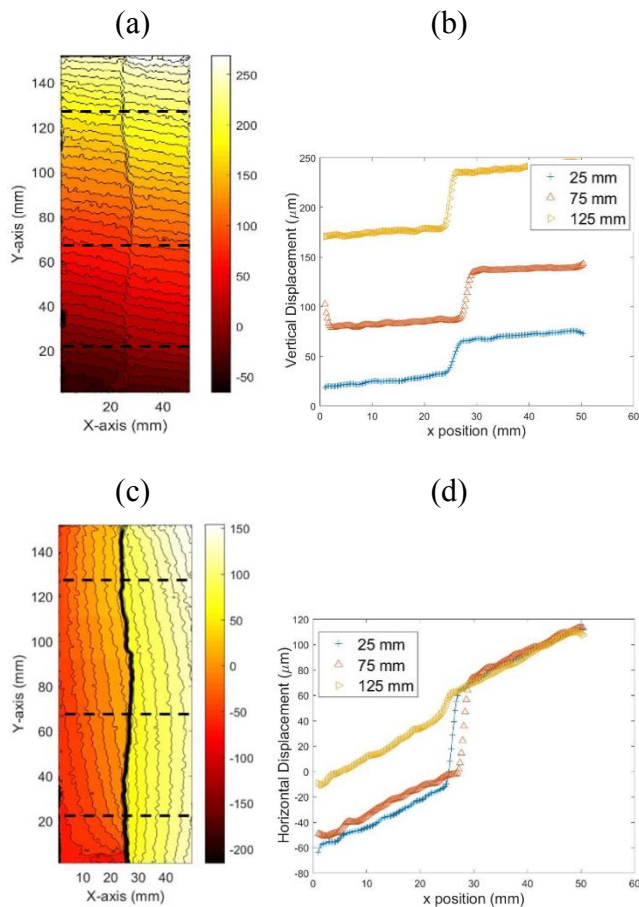


Fig. 12. Specimen G\_1\_125 at peak load; (a) vertical displacement contours; (b) vertical displacements at different horizontal cross-sections; (c) horizontal displacement contours; (d) horizontal displacements at different horizontal cross-sections.

### 3.2. Higher Normal Stress

Experiments were also performed at a high normal stress of 2 MPa on a joint with a half-cycle sine wave with an amplitude of 3.2 mm (Specimen G\_2\_125). Fig. 13 shows the normalized peak-to-peak P and S wave transmitted amplitudes, as well as the shear stress as a function of the shear displacement (for the same representative transducers: top (5S), middle (9P) and bottom (1S) regions of the specimen). The normalized amplitude (for these three transducers) increased with increasing shear strength, then dropped precipitously as the asperities were damaged. Distinct peaks in transmitted wave amplitude were observed prior to shear failure. The observed precursors are associated with peaks in transmitted normalized amplitudes occurring before the peak of the shear strength.

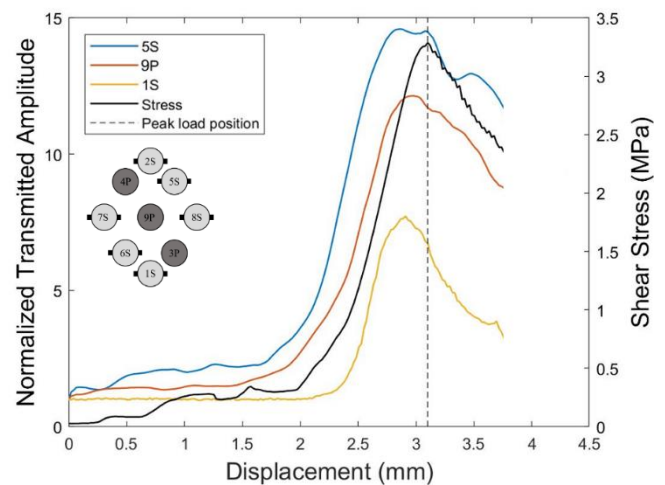


Fig. 13. Shear-stress vs. shear displacement and normalized transmitted amplitude for specimen G\_2\_125, showing representative transducers from top, middle and bottom portion of the sample (shear stress to normal stress ratio=3.41).

Fig. 14 shows the vertical and horizontal displacements recorded at peak load (3.41 MPa). Vertical displacements along the horizontal cross sections ( $y=25$  mm,  $y=75$  mm, and  $y=125$  mm) are presented in Fig. 14(b). Slip (vertical displacement jumps) is observed along the entire contact surface. Fig. 14(c) shows a contour plot of the horizontal displacements, which are displayed in more detail in Fig. 14(d) for the three horizontal lines. Dilation occurred uniformly along the contact surface, which is quite different than what was observed for the same surface profile geometry under lower confinement (Fig. 12(d)). No rotation of the blocks is observed under higher confinement. This, again, is consistent with the recorded normalized transmitted wave amplitudes that all showed a distinct peak and subsequent drop in amplitude.

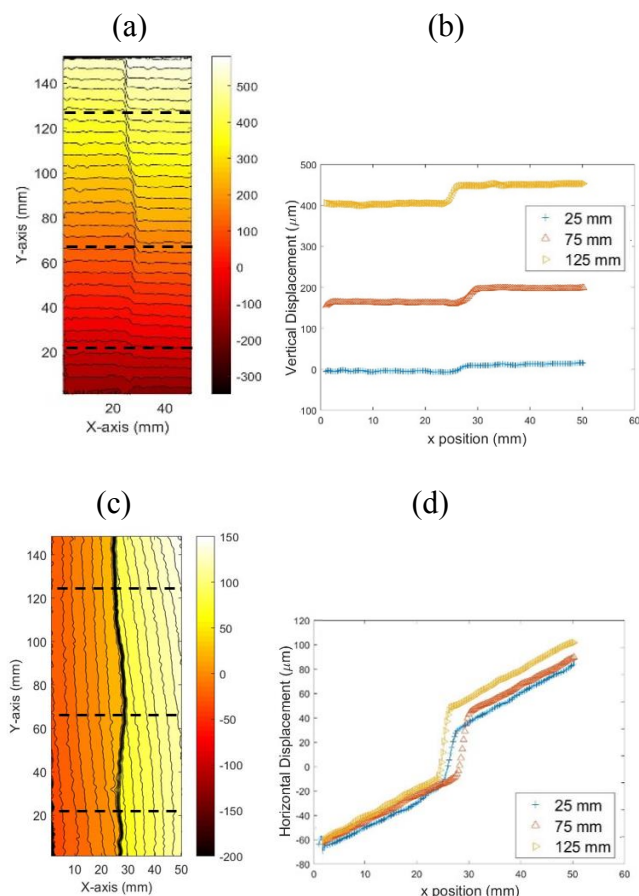


Fig. 14. Specimen G\_2\_125 at peak load; (a) vertical displacement contours; (b) vertical displacements at different horizontal cross-sections; (c) horizontal displacement contours; (d) horizontal displacements at different horizontal cross-sections.

#### 4. CONCLUSIONS

One of the most important implications of this study is that the condition of a joint during shearing can be monitored with compressional and shear waves. It has been observed that the presence of a half-cycle sine wave that has an amplitude of the same order as the size of the asperities yields the same precursors to failure as a planar fracture. Moreover, the shear behavior of a discontinuity is not affected unless the half-cycle sine wave amplitude is at least one order of magnitude larger than the first order asperities. These observations suggest that changes in compressional and shear amplitudes of transmitted waves during shearing are sensitive to the roughness of the joint interface. In addition, the sensitivity to shearing depends on the amount of dilatation that occurs along the interface which is affected by the normal stress on the joint. The experimental results show that changes in transmitted seismic waves may provide a potential method to detect dilatation (and closure) along rock discontinuities, which may prove helpful in assessing key mechanical processes such as the evolution of joint permeability during shearing.

#### ACKNOWLEDGEMENTS

The research presented in this paper is supported by the National Science Foundation, award number: CMMI-1664562. This support is gratefully appreciated.

#### REFERENCES

1. Barton, N. 1973. Review of a new shear-strength criterion for rock joints. *Engineering geology*, 7(4), pp.287-332.
2. Barton, N. and V. Choubey. 1977. The shear strength of rock joints in theory and practice. *Rock mechanics*, 10(1-2), pp.1-54.
3. Choi, M.-K., L.J. Pyrak-Nolte, and A. Bobet. 2014. The Effect of Surface Roughness and Mixed-mode Loading on the Stiffness Ratio  $K_x/K_y$  for Fractures. *Geophysics*, DOI 10.1190/GEO2013-0438.1
4. Giachetti, A. 2000. Matching techniques to compute image motion. *Image and Vision Computing*, 18(3), 247-260.
5. Hedayat, A., L.J. Pyrak-Nolte, and A. Bobet. 2014. Seismic Precursors to the Shear Failure of Rock Discontinuities, *Geophysical Research Letters*, 41:5467-5475 DOI: 10.1002/2014GL060848.
6. Homand, F., T. Belem, and M. Souley. 2001. Friction and degradation of rock joint surfaces under shear loads. *International Journal for Numerical and Analytical Methods in Geomechanics*, 25(10), pp.973-999.
7. Jaeger, J. C., N. G. W. Cook, and R. W. Zimmerman. 2007, *Fundamentals of Rock Mechanics*, Wiley Blackwell, London, U. K.
8. Kendall, K. and D. Tabor. 1971. An ultrasonic study of the area of contact between stationary and sliding surfaces. *Proceedings of the Royal Society of London. A. Mathematical and Physical Sciences*, 323(1554), pp.321-340.
9. Kulatilake, P.H.S.W., G. Shou, T.H. Huang, and R.M. Morgan. 1995, October. New peak shear strength criteria for anisotropic rock joints. In *International Journal of Rock Mechanics and Mining Sciences & Geomechanics Abstracts* (Vol. 32, No. 7, pp. 673-697). Pergamon.
10. Modiriasari, A., A. Bobet, and L. J. Pyrak-Nolte. 2015. Monitoring of Mechanically-Induced Damage in Rock using Transmission and Reflection Elastic Waves. In *the proceeding of the 49th American Rock Mechanics Association, San Francisco, June 29th - July 1st 2015*.
11. Modiriasari, A., A. Bobet, and L.J. Pyrak-Nolte. 2017. Active Seismic Monitoring of Crack Initiation, Propagation, and Coalescence in Rock. *Rock Mechanics and Rock Engineering*, 50, 2311-2325.
12. Mutlu, O. and A. Bobet. 2006. Slip propagation along frictional discontinuities. *International Journal of Rock Mechanics and Mining Sciences*, 43, 860-876.

13. Pan, B., K. Qian, H. Xie, and A. Asundi. 2009, Two-dimensional digital image correlation for in-plane displacement and strain measurement: *A review*, *Meas. Sci. Technol.*, 20, 062001, doi:10.1088/0957-0233/20/6/062001.
14. Patton, F.D. 1966. Multiple modes of shear failure in rock. In *1st ISRM Congress. International Society for Rock Mechanics and Rock Engineering*.
15. Schoenberg, M., 1980. Elastic wave behavior across linear slip interfaces. *The Journal of the Acoustical Society of America*, 68(5), pp.1516-1521.
16. Scrivens, W. A., Y. Luo, Michael A. Sutton, S. A. Collette, Micheal L. Myrick, P. Miney, P. E. Colavita, Anthony P. Reynolds, and Xiaodong Li. "Development of patterns for digital image correlation measurements at reduced length scales." *Experimental Mechanics* 47, no. 1 (2007): 63-77.
17. Sutton, M. A., J.H. Yan, V. Tiwari, H.W. Schreier, & J.J. Orteu. 2008. The effect of out-of-plane motion on 2D and 3D digital image correlation measurements. *Optics and Lasers in Engineering*, 46(10), 746-757.
18. Sutton, M. A., J. J. Orteu, and H. Schreier. 2009. *Image Correlation for Shape, Motion and Deformation Measurements: Basic Concepts, Theory and Applications*. Springer Science & Business Media, p. 342.
19. Zhao, J., 1997a. Joint surface matching and shear strength part B: JRC-JMC shear strength criterion. *International Journal of Rock Mechanics and Mining Sciences*, 34(2), pp.179-185.
20. Xia, C.C., Z.C. Tang, W.M. Xiao, and Y.L. Song, 2014. New peak shear strength criterion of rock joints based on quantified surface description. *Rock Mechanics and Rock Engineering*, 47(2), pp.387-400.